Optimal Selection of Telescope Parameters for Space Situational Awareness Astrometry and Photometry

Timothy S. Murphy
L3 Applied Defense Solutions
Marcus J. Holzinger
University of Colorado Boulder

Abstract

This work proposes a methodology for optimally selecting telescope mount and camera parameters when taking data for space situational awareness applications with various objectives. The primary objectives examined in this work are maximizing information of object location and speed in an image, and information on object brightness over time. The design variables are the telescope integration times over a series of images, the mount angular rates, and camera gain. Constraints include the data downlink rate, pixel saturation, and star field clutter. The final problem is a multi-objective optimization problem with a series of constraints and a variable length vector in the form of the exposure times. The simulation work analyzes the various reward functions individually and the combined Pareto surface.

I. Introduction

THE space domain awareness (SDA) mission continues to require increased efficiency for catalog upkeep and catalog expansion [1]. As the Space Surveillance Network expands, increased numbers of sensors will become available, allowing for more complex operations. Measurements are taken through a variety of phenomenology, but this work is specialized in electro-optical sensors (EOS), that is, telescopes and cameras. These sensors are used to measure light passively reflecting off of space objects. This gives measurements on the space object location and spin state, by measuring the position of the object in the sky and the photometric flux from the object over time.

Telescope operators, when performing SSA missions, have a variety of parameters which must be chosen. This includes exposure time, gain and gamma, exact pointing and slew rate, and in some cases bore sight rotation [2]. These parameters can have large impact on data efficacy, but are often chosen in an ad-hoc manner [3]. From the perspective of research, the telescope is often modeled academically as a sensor which is pointed towards a location in the sky, and obtains measurements on sufficiently bright objects. To the authors knowledge, telescope parameters have never been rigorously explored for SSA specific problems.

This paper treats the telescope tasking problem as a multi-objective optimization problem. The telescope parameters in question are the design variables for this problem, while the objectives are "good" astrometry and photometry. Constraints are introduced by calling out situations which would corrupt data beyond use or be physically impossible.

A. Background

In typical SSA data a series of stationary or moving point sources exist in an image over an integration time. The image shows each point or line blurred by a point spread function, a combination of the airy disc diffraction pattern and other random processes such as atmospheric blur, camera jitter, and photo-electronic bleeding [2] [4] [5]. These processes can produce varied spacial distributions depending on the specific situation, but are often approximated as Gaussian [6]. Various other statistical variation can exist and be quantified for a particular sensor [7].

Astrometry is the process of locating where a point source exists in the field of view of a sensor. This is a relevant problem in SSA, astronomy, microscopy, and other fields, and is accomplished through various techniques including thresholding, calculating a centroid, or maximum likelihood estimation. In particular, the maximum likelihood detection method is seen as a statistically rigorous method for making sensitive detection [8], [9], [10] and has grown in popularity recently for SSA applications [11]. Maximum likelihood detection is a method for estimating specific parameters by optimally choosing an estimate that most closely matches received data. In other words, an estimate is chosen by minimizing residuals relative to their specific variances. This method incorporates pixel-to-pixel data in the images and works along the same principles as a matched filter [12]. In astronomy, from which many SSA methods are derived, object motion is virtually non-existent and limits on exposure time are less critical. For SSA, good estimates on both space objects position and velocity in the image plane are desired. Objects may be rate tracked or allowed to streak through an image; maximum likelihood estimation on moving objects is an area which has been explored but in less detail than stationary objects [13]. In this paper, astrometry then refers to measuring the position of an object in an image and the velocity of an object through the image.

One of the techniques which uses image data is categorization and intent characterization of space objects. This can include resolved imagery which looks to use pixel information to match an image to a shape model, but this type of work is not looked at in this paper. Instead, this paper focuses on point sources, where the only information is how much light is received from an object. Light curve inversion is a newer method in SSA which looks at identifying the shape and properties on a space object based on the light curve [14] [15]. These techniques are based on methods developed for identifying the approximate shape of asteroids [16],[17]. This can look at trying to estimate the shape model of a completely unknown object. Previous work also suggests that with a shape model, a light curve can indicate the type of mission the object may have [18]. For all of these missions, the data input into the estimation technique is time resolved flux information. These methods should be improved by both denser time resolution of the flux and more accurate estimation of the flux values. The optimization in this paper focuses on these two factors.

B. Methodology

This paper develops a framework of how to choose tasking parameters for taking electro-optical SSA data. Specific reward functions are developed for position, velocity, and brightness of a point sources. This includes a novel derivation of point source velocity information and time varying photometry aliasing bias. Each of these reward functions are extended to a streaking object as well. Timing uncertainty is incorporated into the reward functions. The gradients with respect to exposure times are developed for all reward functions to ease analysis and optimization. Several constraint on how data can be taken are included to ensure optimization solutions are realistic. Finally, simulation work provides a blueprint on how to solve such optimization problems while providing insight into what general properties an optimal campaign has.

In section II the optimization problem is set up. First, the various available design variables are defined and discussed. The statistics of image and point source data form the groundwork of this paper and are succinctly introduced. A few other background topics are discussed as well.

Section III introduces the three main reward functions in this paper. First, maximum likelihood estimation on an image is introduced along with a general formula for Fisher information. The astrometric information for both position and velocity is presented. Both these functions are developed for both a stationary and streaking object. Timing uncertainty is also incorporated into these reward functions. A formulation for photometry information is developed, which incorporates flux bias from rapidly changing signals.

Section IV finishes defining the optimization problem by discussing various constraints. This includes side constraints for variables and physical constraints for a telescope system such as pixel saturation and pixel bleeding. More interestingly, star background clutter is analyzed as a constraint, providing an analytic way to trade off information gain from long exposures with potential information loss from objects intersecting stars.

Section V discusses the various optimization techniques used in this paper. First, gradients for each of the reward functions are developed, which provide both insight into how the reward functions behave and a faster way to solve the optimization problem. More advanced gradients are also developed in Appendix A. The Karush Kuhn Tucker conditions are briefly discussed in this section. Finally, a loose outline of how the single objective and multi-objective optimizations are solved is presented. This includes a discussion of some of the hurdles and pitfalls in the optimization process.

Finally, Section VI analyzes the various reward functions in simulation. First each reward function is solved by itself. Discussions on the general shape of solutions along with intuitive analysis of the behavior of the reward functions are included. The combined multi-objective optimization process is also analyzed, with the inclusion of both a Pareto surface and sample solutions along the surface.

II. Optimization Set Up

This section, in order, define the design variables, objectives, and constraints of the optimization problem.

A. Available Design Variables

Before the definitions and behaiviors of the various SSA objectives can be analyzed, and list of designable variables is needed.

First, the camera integration time is defined. Integration time, t_I, also known as exposure time, is the amount of time spent collecting photons for a single image. Longer integration time implies more photons are collected which implies higher informational content. This obtains better centroids leading to more precise astrometry. Longer exposure time also leads to higher probability of detection in a particular frame. Shorter integrations leads to more images over a set period of time which gives more temporal information. Some photometry missions attempt reconstruction of highly variable light curves over time, while velocity information in images needs some element of temporal information.

In general, this paper assumes multiple images may be taken, each with its own integration time. This forms a rather unique design variable, a variable length vector, $\mathbf{t} \in \mathbb{R}^{N_t+1}$. To aid this discussion, refer to Figure 1 for clarification. This paper uses the start times of each integration, t_k, as the design variable and models the rest of the timing quantities around it. Sensors

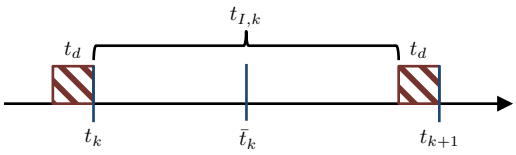

Fig. 1. Various variables associated with time during a series of integrations.

require some time to upload pixel information between integrations, which is modeled as a constant dead time, t_d, seen in Figure 1. Then the kth integration is defined as

$$t_{I,k} = t_{k+1} - t_k - t_d \tag{1}$$

Note that in this formulation the first element t_1 is always zero and a final t_{N_t+1} must also be included. Even though there are $N_t + 1$ elements, the first and last are always fixed so there are only $N_t - 1$ variables to optimize over. As mentioned, the is a variable length vector in that N_t can be varied and whatever optimization method used must be able to handle this. Finally, the center time of each integration is useful to define for future discussions as the midpoint of a particular integration,

$$\bar{t}_k = (t_k + t_{k+1} - t_d)/2 \tag{2}$$

which can also be seen in Figure 1.

Next, two continuous variables, $\alpha(t)$ and $\delta(t)$ are defined. This paper treats these variables as the inertial angles, right ascension and declination, but they could just as easily represent a unit vector or local frame (e.g. azimuth and elevation). These variables need to be defined over the exposure time taken by a sensor. In many cases, this leads to defining four parameters $[\alpha(t_0), \delta(t_0), \dot{\alpha}(t_0), \dot{\delta}(t_0)]$. This can be further simplified by moving the variables into the image plane as $[x(t_0), y(t_0), \dot{x}(t_0), \dot{y}(t_0)]$. Finally, it is worth noting that $x(t_0)$ and $y(t_0)$ are mostly immaterial as design variable because they only determine where in the image an object shows up; they do not affect information the brightness or shape of the object. This paper assumes the object is in the field of view and there is insignificant distortion in the sensor to affect information, which may not be true for very wide fields of view. Better rate tracking of an object concentrates more light into fewer pixels, increasing probability of detection and photometry information. Astrometry, however, can be improved in certain situations by imperfect rate tracking, depending on the exact mapping between the point spread function and pixel space.

Next, the gain map must be discussed. This consists of an overall gain, G, and a gamma filter, Γ. These effect the mapping of electrons on a CCD to pixel values. If chosen incorrectly pixel saturation occurs distorting and biasing photometry information. However, on the other end, very dim signals can have very poor discretization.

B. Image Statistics

This section defines statistical models for an image that are used throughout the paper. An image is made up of a series of pixel measurements broken into deterministic signal content and zero mean noise of known distribution (assuming background subtraction has been performed [19]),

$$z_i = s_i + w_i \tag{3}$$

$$w_i \sim p(w_i), \ \mathbb{E}[w_i] = 0 \tag{4}$$

where $p(w)$ is some PDF or probability mass function (PMF) of known form, and i is an index denoting a particular pixel.

A good way to model the statistics of a pixel is with a series of Poisson distributions [20]. The pixel is composed of signal (shot noise), dark noise, and read noise which are all Poisson distributed. The dark and read noise can be combined into one Poisson distributed random variable with parameter, $\lambda_{w,i}$, while the shot noise has parameter $\lambda_{s,i}$. It is convenient to factor out the mean of the shot noise as signal, s_i, and subtract out the mean of the remaining noise, which gives new definitions to the variables in (3),

$$s_i = \lambda_{s,i} \tag{5}$$

$$w_i \sim \{\mathcal{P}(\lambda_{w,i} + \lambda_{s,i}) - (\lambda_{w,i} + \lambda_{s,i})\} \tag{6}$$

However, there are more simplifications which are often used. A Poisson distribution approaches a Gaussian distribution as λ increases [21]. Furthermore, for bright objects the contribution of shot noise on total system randomness is often ignored and read noise is mostly constant within a small region of pixels. The final formulation of a pixel, which is used throughout this paper, is then

$$z_i = s_i + w_i \tag{7}$$

$$s_i = \lambda_{s,i} \tag{8}$$

$$w_i \sim \mathcal{N}(0, \sigma_i^2) \tag{9}$$

where $\sigma_i^2 = \lambda_{w,i}$. Note that the Fisher information for Poisson distributed pixels is derived in the same way as that of Gaussian pixels [9]. The work presented in this paper can therefore by generalized to explicitly Poisson noise as well.

It is important to understand that measurements taken over the kth integration time are dependent on the length of the integration time along with a series of other factors. The expected value of the noise, which is equal to the variance due to the underlying Poisson distribution, is

$$\lambda_{w,i} = \sigma_i^2 = GQ\delta^2 F_o t_{I,k} = BF_o t_{I,k} \tag{10}$$

where Q is the quantum efficiency, δ^2 is the area of each pixel, and F_o is the background and dark current flux rate. In the final line, the constants are wrapped into the parameter $B = \delta^2 GQ$ to ease notation. This implies that the design variable vector $\mathbf{t}$ affects the information content directly through changing the background variance.

III. Reward Functions for SSA

A. Maximum Likelihood Estimator

For the purposes of this paper, an estimator needs to be constructed for the flux, position and velocity of a space object at some time $\theta = (F, x^*(t^*), y^*(t^*), \dot{x}^*(t^*), \dot{y}^*(t^*))$. Note that the position and velocity shown above are treated as the location and velocity of the center (mean) of a point light source in the image plane. A point source object spreads over pixels through a spatial PDF, $h(\mathbf{x}_{i,k}|t)$, called a point spread function (PSF), where $\mathbf{x}_{i,k} = [x_{i,k}, y_{i,k}]^T$ is a specific pixel coordinate. Under ideal conditions the PSF is an Airy disc [5], but is often approximated as Gaussian. In reality, this function is disturbed by atmospheric distortion and mount jitter as well, further distributing the light. The PSF spatial distribution is then

$$h(\mathbf{x}_{i,k}|t_k) = \frac{1}{\sqrt{(2\pi w^2)^2}} e^{-(\xi_{i,k}^2 + \eta_{i,k}^2)/2w^2} \tag{11}$$

$$\xi_{i,k} = (x_{i,k} - x_k^*), \;\; \eta_{i,k} = (y_{i,k} - y_k^*) \tag{12}$$

$$x_k^* = x^*(t^*) + \dot{x}^*(t^*)(t_k - t^*) \tag{13}$$

$$y_k^* = y^*(t^*) + \dot{y}^*(t^*)(t_k - t^*) \tag{14}$$

where w^2 is the variance of the point spread function. Note that the location of the point source in the image is defined through a series of constants to be estimated, $x^*(t^*), y^*(t^*), \dot{x}^*(t^*), \dot{y}^*(t^*)$, and the time t_k. This final PSF $h(\mathbf{x})$ describes the spatial probability density of photons hitting the ccd plane.

The photons coming off of an object, entering the aperature of a telescope, and hitting the CCD can be described as a Poisson process and distribution, $P(\lambda)$. Each photon goes through a series of random events, including hitting a random place on the CCD (PSF, $h(\mathbf{x})$), having a random chance at not being detected (Quantum Efficiency, Q), and being converted in batches to pixel counts (Gain, G). Each pixel can be then be described as a Poisson distribution, and approximated as Gaussian as in (7). The expected number of pixel counts (parameter of the Poisson distribution) for pixel i and timestep k is

$$\begin{aligned} s_{i,k} = \lambda_{i,k} &= G\,Q\,F\,t_{I,k} \int_{\text{pixel}} h(\mathbf{x})\mathrm{d}\mathbf{x} \\ &\approx G\,Q\,F\,t_{I,k}\,\delta^2 h(\mathbf{x}_{i,k}) \\ &= \frac{Bt_{I,k}F}{\sqrt{(2\pi w^2)^2}}\, e^{-(\xi_{i,k}^2 + \eta_{i,k}^2)/2w^2} \end{aligned} \tag{15}$$

where F is the (average) photon rate off of the object entering the aperture in photons per second and the integral calculates the probability a given photon hits pixel i. In reality, the PSF should be integrated over the pixel, but the approximation in line 2 is a common simplification [9] and effectively a linear approximation of the integral.

Each pixel also has further corruptions from dark current and read noise which can both be modeled as Poisson and approximated as zero mean Gaussian. Each pixel has a distribution of

$$p(z) = \frac{1}{\sqrt{2\pi\sigma_{i,k}^2}} e^{-(z - s_{i,k})^2/2\sigma_{i,k}^2} \tag{16}$$

where $s_{i,k}$ is the expected signal value. Note that it is common to approximate this distribution as Gaussian, so long as the expected value is high enough. The entire process can be seen, nominally, in Figure 2.

Precise astrometry can be calculated in a variety of ways, but this paper looks at the commonly used maximum likelihood estimator [9]. The astrometry can be evaluated through how well the covariance matrix of the measurement is minimized.

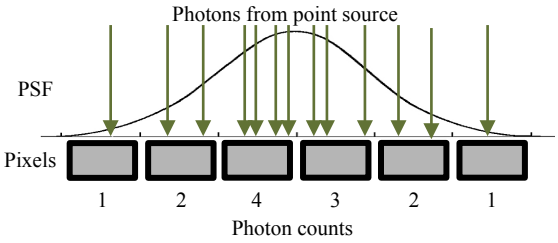

Fig. 2. Photons from a point source are randomly distributed across pixels according to a point spread function. Number of photons is determined randomly via a Poisson distribution.

Similarly, this can be seen as maximizing the Fisher information in the estimator [22]. The derivation of the Fisher information starts with the log likelihood function, $l(\theta) = \log(L(\theta|\mathbf{z})) = \log(p(\mathbf{z}|\theta))$, which for this example is

$$l(\theta) = \sum_{k=1}^{N_t} \sum_{i=1}^{N_k} \log\left(\frac{1}{\sqrt{2\pi\sigma_{i,k}^2}}\right) + \left(\frac{-(z_{i,k} - s_{i,k})^2}{2\sigma_{i,k}^2}\right) \tag{17}$$

Note that the summation over k and i are combined and dropped in future equations for ease of notation, but in general all summations occur over both k and i. Also note that N_k is a function of the time step k. Then the first derivative is generally

$$\frac{\partial l(\theta)}{\partial \theta_j} = \sum \frac{1}{\sigma_{i,k}^2}(z_{i,k} - s_{i,k})\frac{\partial s_{i,k}}{\partial \theta_j} \tag{18}$$

The Fisher information is found by taking the expected value of the square of the gradient above. Future sections calculate fisher information for a variety of values of θ_j.

B. Streaking Object Point Spread Function

This section quantifies the modified point spread function, $\tilde{h}(\mathbf{x}_i)$, for a streaking object. The goal is to modify the PSF in (15) for a streaking object. The primary difference is explicitly integrating over the integration time rather than just including $t_{I,k}$,

$$\begin{aligned} t_{I,k}\tilde{h}(\mathbf{x}_{i,k}|t) &= \int_{t_k}^{t_{k+1}-t_d} h(\mathbf{x}_{i,k}|t)\mathrm{d}t \\ &= \int_{t_k}^{t_{k+1}-t_d} \frac{1}{\sqrt{(2\pi w^2)^2}} e^{-(\xi_{i,k}^2(t)+\eta_{i,k}^2(t))/2w^2}\mathrm{d}t \end{aligned} \tag{19}$$

where $\xi_{i,k}$ and $\eta_{i,k}$ are now time dependent implying h must be explicitly integrated. Note that $t_{I,k}$ must be included as part of the definition, because it is calculated through the integral.

There is a useful shortcut in the evaluation of the integral in (19). In order ease this calculation, this integral can be reparameterized into the distance parallel and orthogonal to the motion of the Gaussian, $[\dot{x}^*, \dot{y}^*]^T$, which are internal parameters in h. Note that while the parallel distance, $\tilde{\xi}$, is time varying the orthogonal distance, $\tilde{\eta}$, is time invariant. Then the same integral is

$$t_{I,k}\tilde{h}(\mathbf{x}_{i,k}|t) = \frac{e^{-\tilde{\eta}_{i,k}^2/2w^2}}{\sqrt{(2\pi w^2)^2}} \int_{t_{I,k}}^{t_{I,k+1}} e^{-\tilde{\xi}_{i,k}^2(\tilde{x}(t))/2w^2}\mathrm{d}t \tag{20}$$

where one direction of the Gaussian is removed from the integral and the other is calculated from a simple 1-D Gaussian integral evaluation.

C. Astrometry Reward for Space Object Orbit Determination

In order to synthesize a reward function for tasking parameters with respect to astometry, the Fisher information is calculated in this section. Astrometry for space objects in this case is $\theta = (x^*(t^*), y^*(t^*), \dot{x}^*(t^*), \dot{y}^*(t^*))$. The derivation starts with evaluating (18) for the above θ, which leads to

$$\begin{aligned}
\frac{\partial l}{\partial x^*} &= \frac{1}{w^2}\sum \frac{(z_{i,k}-s_{i,k})}{\sigma_{i,k}^2}\xi_{i,k}s_{i,k} \\
\frac{\partial l}{\partial y^*} &= \frac{1}{w^2}\sum \frac{(z_{i,k}-s_{i,k})}{\sigma_{i,k}^2}\eta_{i,k}s_{i,k} \\
\frac{\partial l}{\partial \dot{x}^*} &= \frac{1}{w^2}\sum \frac{(z_{i,k}-s_{i,k})}{\sigma_{i,k}^2}\xi_{i,k}s_{i,k}(\bar{t}_k - t^*) \\
\frac{\partial l}{\partial \dot{y}^*} &= \frac{1}{w^2}\sum \frac{(z_{i,k}-s_{i,k})}{\sigma_{i,k}^2}\eta_{i,k}s_{i,k}(\bar{t}_k - t^*)
\end{aligned} \tag{21}$$

The Fisher information is found by taking the expected value of the square of the gradient above. First note that in this form, the only random variable is the pixel measurements, $z_{i,k}$, which appears once. While the square of (21) is the square of a sum, $\mathbb{E}[(z_{i,k}-s_{i,k})(z_{j,k}-s_{j,k})] = 0$ for $i \neq j$ so long as noise is uncorrelated. For the rest of the terms, $\mathbb{E}[(z_{i,k}-s_{i,k})^2] = \sigma_{i,k}^2$, giving Fisher information results of

$$I_{xx} = \frac{1}{w^4}\sum \frac{\xi_{i,k}^2 s_{i,k}^2}{\sigma_{i,k}^2} \tag{22}$$

$$I_{yy} = \frac{1}{w^4}\sum \frac{\eta_{i,k}^2 s_{i,k}^2}{\sigma_{i,k}^2}$$

$$I_{\dot{x}\dot{x}} = \frac{1}{w^4}\sum \frac{\xi_{i,k}^2 s_{i,k}^2}{\sigma_{i,k}^2}(\bar{t}_k - t^*)^2 \tag{23}$$

$$I_{\dot{y}\dot{y}} = \frac{1}{w^4}\sum \frac{\eta_{i,k}^2 s_{i,k}^2}{\sigma_{i,k}^2}(\bar{t}_k - t^*)^2$$

Next, the same calculation is made for a moving point spread function. The moving point spread function in (19) can be plugged directly into the second line of (15). Referencing (18), the same derivative is calculated which for position and velocity information is unaffected by the presence of an integral over time.

$$\frac{\partial l}{\partial x^*} = \frac{BF}{w^2}\sum \frac{(z_{i,k}-s_{i,k})}{\sigma_{i,k}^2}\int_{t_k}^{t_{k+1}-t_d} \xi_{i,k}h_{i,k}\mathrm{d}t \tag{24}$$

$$\frac{\partial l}{\partial \dot{x}^*} = \frac{BF}{w^2}\sum \frac{(z_{i,k}-s_{i,k})}{\sigma_{i,k}^2}\int_{t_k}^{t_{k+1}-t_d} \xi_{i,k}h_{i,k}(t-t^*)\mathrm{d}t \tag{25}$$

which turns into the position and velocity information

$$I_{xx} = \frac{B^2F^2}{w^4}\sum \frac{1}{\sigma_{i,k}^2}\left(\int_{t_k}^{t_{k+1}-t_d} \xi_{i,k}h_{i,k}\mathrm{d}t\right)^2 \tag{26}$$

$$I_{\dot{x}\dot{x}} = \frac{B^2F^2}{w^4}\sum \frac{1}{\sigma_{i,k}^2}\left(\int_{t_k}^{t_{k+1}-t_d} \xi_{i,k}h_{i,k}(t-t^*)\mathrm{d}t\right)^2 \tag{27}$$

In affect, the streak information only requires calculating the modified expected value of each pixel. These integrals can be easily calculated for each pixel through a Riemann approximation.

D. Photometry Reward for Space Object Characterization

First, the information on the estimate of the photometric flux, that is, how accurately the flux is estimated in an image, is shown. Starting with (18),

$$\frac{\partial l(F)}{\partial F} = \sum \frac{1}{\sigma_{i,k}^2}(z_{i,k}-s_{i,k})Bt_{I,k}h(\mathbf{x}_{i,k}) \tag{28}$$

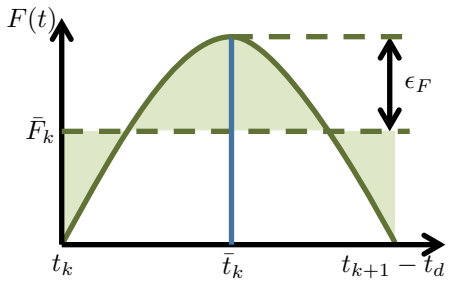

Fig. 3. An inherent bias, ϵ_F, is created when observing a fluctuating signal.

where the F in the denominator cancels with the F in $s_{i,k}$. To get the information, the expectation of the square of (28) is required,

$$I_{FF} = B^2 \sum \frac{t_{I,k}^2 h(\mathbf{x}_{i,k})^2}{\sigma_{i,k}^2} \tag{29}$$

1) Photometry Bias: For a time varying photometric flux signature, the point spread function must be integrated over time.

$$\begin{aligned} s_{i,k} &= G \int_{t_k}^{t_{k+1}-t_d} F(t) \int_{\text{pixel}} h(\mathbf{x}) \mathrm{d}\mathbf{x} \mathrm{d}t \\ &\approx B t_{I,k} \bar{F} h(\mathbf{x}_{i,k}) \end{aligned} \tag{30}$$

The flux is only observed through $\bar{F}$, the average flux over the integration time. Because average flux over a time period is a difficult measurement to incorporate into an estimation scheme, the measurement is often treated as the instantaneous flux at the central time, $\bar{t}_k$. For flux that varies linearly over the integration time, this assumption is accurate, but many real scenarios can contain significantly varying signals. Furthermore, the variations in flux are often an important piece of information in object characterization. These variations provide an inherent bias, ϵ_F, in the photometric measurements, which is illustrated in Figure 3.

The expected value of the pixels are then

$$s_{i,k} = B t_{I,k} (F(\bar{t}_k) + \epsilon_F) h(\mathbf{x}_{i,k}) \tag{31}$$

where $\bar{F}$ is split into the true term to be estimated and a bias error term, ϵ_F. The bias is dependent on the shape of the signal itself, thus to make further progress a model for the flux is proposed. Typically, the kind of quick flux changes which occur during an integration are due to periodic variations on flux. The flux is modeled as a sum of sinusoidal signals. It is also assumed that if the highest frequency signal is sampled sufficiently, all lower frequency signals are also sufficiently sampled. Therefore, the goal of photometry is to sufficiently sample

$$F(t) = F_0 + A \sin(\omega t + \theta) \tag{32}$$

where F_0 is the average flux, θ is the phase shift, and A and ω are the amplitude and frequency of the highest frequency time varying component. The bias is then

$$\begin{aligned} \epsilon_F &= F(\bar{t}_k) - \frac{1}{t_{I,k}} \int_{t_k}^{t_{k+1}-t_d} F(t) \mathrm{d}t \\ &= A \sin(\omega \bar{t}_k + \theta) - \frac{1}{t_{I,k}} \int_{t_k}^{t_{k+1}-t_d} A \sin(\omega t + \theta) \mathrm{d}t \end{aligned} \tag{33}$$

For further analysis, it would be useful to quantify the distribution of ϵ_F. The unknown phase shift, θ, is uniformly distributed over $\mathbb{R}$ but, due to the cyclical nature of the $\sin$ function, can be assumed as uniformly distributed over $[0, 2\pi]$. For the timing

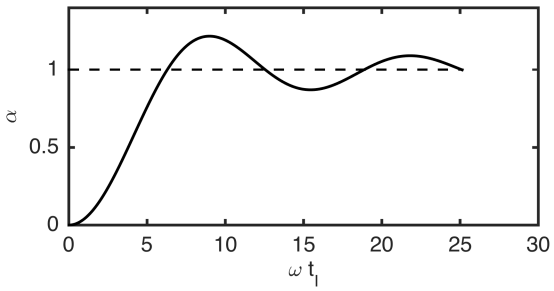

Fig. 4. Variation of α with respect to the time constant $\omega t_{I,k}$ with constant $A = 1$.

$\bar{t}_k$, t_k, and t_{k+1} can be assumed as any given choice simply shifts $\omega\bar{t}_k + \theta$, which is still uniform over one cycle of $\sin$. Applying these assumptions and a change in variable, $\tau = \omega t$, gives

$$\begin{aligned}\epsilon_F &= A\left(\sin(\theta) - \frac{1}{t_{I,k}}\int_{-t_{I,k}/2}^{t_{I,k}/2}\sin(\omega t+\theta)\mathrm{d}t\right)\\ &= A\left(\sin(\theta) - \frac{1}{\omega t_{I,k}}\int_{-\omega t_{I,k}/2}^{\omega t_{I,k}/2}\sin(\tau+\theta)\mathrm{d}\tau\right)\end{aligned} \tag{34}$$

where $\omega t_{I,k}$ forms a time factor. As $\omega t_{I,k} \to 0$, the right side of the equation becomes a very accurate estimate of $\sin(\theta)$ which drives $\epsilon_F \to 0$. As $\omega t_{I,k} \to \infty$, the integral becomes cyclical between -1 and +1, and so $\epsilon_F \to \sin(\theta)$. This integral can be evaluated directly, giving

$$\begin{aligned}\epsilon_F =& A\Bigg(\sin(\theta) + \frac{1}{\omega t_{I,k}}\cos(\theta+\omega t_{I,k}/2)\\ &- \frac{1}{\omega t_{I,k}}\cos(\theta-\omega t_{I,k}/2)\Bigg)\end{aligned} \tag{35}$$

which can be simplified with the half angle formula into

$$\begin{aligned}\epsilon_F &= A\sin(\theta)\left(1 - \frac{2}{\omega t_{I,k}}\sin(\omega t_{I,k}/2)\right)\\ &= \alpha\sin(\theta)\end{aligned} \tag{36}$$

where α is the modified amplitude

$$\alpha = A\left(1 - \frac{2}{\omega t_{I,k}}\sin(\omega t_{I,k}/2)\right) \tag{37}$$

Note that the phase still heavily affects the bias through the $\sin(\theta)$ and the results as $\omega t_{I,k}$ goes to zero or infinity still hold. Finally, if θ is uniformly distributed,

$$p_{\text{asin}}(\epsilon_F;\alpha) = \frac{1}{\pi\sqrt{\alpha^2-\epsilon_F^2}} \tag{38}$$

giving a PDF for the flux bias. This distribution is the symmetric case of the arcsine distibution. The expected value is zero which intuitively makes sense, and the variance is

$$\begin{aligned}\mathrm{Var}(\epsilon_F) &= \int \epsilon_F^2\frac{1}{\pi\sqrt{\alpha^2-\epsilon_F^2}}\mathrm{d}\epsilon_F\\ &= \alpha^2/2\end{aligned} \tag{39}$$

which can be analytically calculated.

2) High Frequency Photometry: Now the photometric information can be calculated with the bias, ϵ_F, taken into account. Because the bias is inherently stochastic and unknown, the best available estimate of the expected value in each pixel is still (15), where F is the instantaneous flux. However, each pixel has an added stochastic term

$$\begin{aligned} z_{i,k} &= B(F+\epsilon_F)t_{I,k}h(\mathbf{x}_{i,k}) + w_{i,k} \\ &= s_{i,k} + B\epsilon_F t_{I,k}h(\mathbf{x}_{i,k}) + w_{i,k} \end{aligned} \tag{40}$$

$$\epsilon_F \sim p_{\text{asin}}(\alpha), w_{i,k} \sim \mathcal{N}(0, \sigma_{i,k}^2) \tag{41}$$

$$\text{Var}(z_{i,k}) = \sigma_{i,k}^2 + (B^2 t_{I,k}^2 \alpha^2 h_{i,k}^2)/2 \tag{42}$$

In order to incorporate this into the Fisher information, (18) is evaluated for the new distribution,

$$\begin{aligned} \frac{\partial l(F)}{\partial F} &= B\sum \frac{(z_{i,k}-s_{i,k})}{\text{Var}(z_{i,k})} t_{I,k}h_{i,k} \\ \frac{\partial l(F)}{\partial F} &= B\sum \frac{(w_{i,k}+B\epsilon_{F,k}h_{i,k})}{\text{Var}(z_{i,k})} t_{I,k}h_{i,k} \end{aligned} \tag{43}$$

noting that $\epsilon_{F,k}$ is invariant over index i. To get information, the expectation of the square of is required, but unlike before, cross terms are not necessarily uncorrelated,

$$I_{FF} = B^2\mathbb{E}\left[\left(\sum_k\sum_i (w_{i,k}+B\epsilon_{F,k}h_{i,k})\frac{t_{I,k}h_{i,k}}{\text{Var}(z_{i,k})}\right)^2\right] \tag{44}$$

where $w_{i,k}$ and $\epsilon_{F,k}$ are the only stochastic terms. Note that while the various $w_{i,k}$ are uncorrelated with each other and $w_{i,k}$ is uncorrelated with $\epsilon_{F,k}$, there are $\epsilon_{F,k}\epsilon_{F,l}$ which are correlated based on their time offset by the term $\cos(\omega(\bar{t}_k - \bar{t}_l))$. In reality this creates a quadruple sum reward function over two time step dimensions and two pixel dimensions. Furthermore, the correlation can be both positive and negative and is based on an initially unknown frequency. For the simulation work, these correlation terms are not included for this reward function giving a simplified information of

$$I_{FF} = B^2\sum_{i,k}\frac{t_{I,k}^2 h_{i,k}^2}{\text{Var}(z_{i,k})} \tag{45}$$

This version of the reward inflates the variance of each pixel with the added uncertainty of ϵ_F.

E. Streaking Photometry

The streaking point spread function is straight forward to calculate. The primary difference is in substituting $\tilde{h}$ in (19) for h,

$$I_{FF} = B^2\sum_{i,k}\frac{\left(\int_{t_k}^{t_{k+1}-t_d} h_i(t)\text{d}t\right)^2}{\text{Var}(z_{i,k})} \tag{46}$$

Note that $\tilde{h}$ also must be substituted into the variance equation.

F. Timing Uncertainty

When considering real optical sensors, there are a variety of other parameters, such as timing uncertainty, which may have inherent uncertainty and therefore affect the information content. This section serves as a template on how to incorporate additional uncertainties into the above reward functions. Additional uncertainty only needs to be introduced into the stochastic measurement variables, $z_{i,k}$, which typically takes the form of inflating the final variance, $\sigma_{i,k}^2$. In the case of timing uncertainty, zero mean Gaussian timing error is added at each time step,

$$\tilde{t}_k = t_k + \epsilon_{t,k}, \qquad \epsilon_{t,k} \sim \mathcal{N}(0, w_t^2) \tag{47}$$

where w_t is the known timing variance. The equations in (22) and (23) are valid then, because the timing uncertainty does not change the expected value of the pixels, only the variance. The pixel variance needs to be updated for the new value of $\sigma_{i,k}^2$ which incorporates timing uncertainty. The primary effect of timing uncertainty occurs through changing the integration time. Using the $\sim$ notation to represent variables which have an internal timing uncertainty,

$$\begin{aligned} \tilde{t}_{I,k} &= t_{k+1} + \epsilon_{t,k+1} - t_k - \epsilon_{t,k} - t_d \\ &= t_{I,k} + \sqrt{2}\epsilon_{t,k} \end{aligned} \tag{48}$$

which gives

$$\begin{aligned} z_{i,k} &= \tilde{s}_{i,k} + w_{i,k} \\ \tilde{s}_{i,k} &= BFh(\mathbf{x}_{i,k})\tilde{t}_{I,k} \\ &= s_{i,k} + \sqrt{2}BFh(\mathbf{x}_{i,k})\epsilon_t \\ z_{i,k} &= s_{i,k} + w_{i,k} + \sqrt{2}BFh(\mathbf{x}_{i,k})\epsilon_t. \end{aligned} \tag{49}$$

For a streaking object, (19) must be used as the basis for describing pixels, so the uncertainty is part of the integral bounds. Considering uncertainty in only t_k for ease on derivation, the integral can be broken into the original component and a small stochastic component,

$$\begin{aligned} z_{i,k} &= \tilde{s}_{i,k} + w_{i,k} \\ \tilde{s}_{i,k} &= BF \int_{t_k+\epsilon_{t,k}}^{t_{k+1}-t_d} h_{i,k}(t)\mathrm{d}t \\ &= s_{i,k} + BF \int_{t_k+\epsilon_{t,k}}^{t_k} h_{i,k}(t)\mathrm{d}t. \end{aligned} \tag{50}$$

If $\epsilon_{t,k}$ is small, which typically is the case, the integral can be linearized around t_k

$$\tilde{s}_{i,k} \approx s_{i,k} + BFh_{i,k}(t_k)\epsilon_{t,k} \tag{51}$$

where $h_{i,k}(t_k)$ is the point spread function at the time t_k. This linearization also depends on a small in plane velocity; the assumption is that the point spread function is effectively stationary over the range of the timing error. Taking into account uncertainty at t_{k+1} as well gives

$$\tilde{s}_{i,k} \approx s_{i,k} + BF(h_{i,k}(t_k)\epsilon_{t,k} + h_{i,k}(t_{k+1})\epsilon_{t,k+1}). \tag{52}$$

First note that the timing uncertainty affects pixels proportionally to the point spread function at that time, $h_{i,k}(t)$. This implies that only pixels near the end points are affected by timing uncertainty.

The timing uncertainty can be incorporated into any of the above reward functions by inflating the variance of each pixel by the additive Gaussian term in (49) or (52) for a stationary or moving PSF respectively. The timing can also affect the information in a second way: by changing exposure time, the mean background radiation is affected as well. This uncertainty is a gray area because effective background subtraction implies that any such variation in background is estimated and removed.

IV. Constraining Parameters

This section outlines the constraints being used for this optimization problem. The standard notation for inequality constraints is as functions $g(x) \leq 0$.

A. Physical Constraints

The first constraint is total time allocated for images, T. The series of N_t images each take their respective integration times to be captured. The camera must upload the pixel information between integrations. This dead time, t_d, occurs $N_t - 1$ times and is a function of the image size and the data transfer rate of the camera. Because of the structure of $\mathbf{t}_I$, this can be implemented as a constraint on the last element of the vector, t_{I,N_t+1}, and is effectively an equality constraint that must be zero.

$$g_t(\mathbf{t}_I) = (N_t - 1)t_d + \sum_{k=1}^{N_t} t_{I,k} - T \tag{53}$$

$$g_t(t_{I,N_t+1}) = t_{I,N_t+1} - T \tag{54}$$

The next constraint is based on pixel saturation and bleeding. When a CCD integration is sufficiently high such that a pixel reaches its maximum number of counts, or FWC (full well capacity), the pixel begins to "bleed" its counts into adjacent pixels [23]. Pixel bleeding adds extra signal over vast areas of an image, with poorly understood statistical distributions, rendering those areas unusable. This paper treats bleeding as unacceptable; even if bleeding in an image does not affect the target being observed, secondary objects may move through an image but be obscured by bleeding. Bleeding is dependent on the number

of photons hitting a pixel and is therefore unaffected by gain. It is also dependent on the flux of the brightest star in the image, F_{max}, which must therefore be predicted or estimated. This leads to

$$g_b(t_{I,k}) = \frac{F_{\text{max}}\, t_{I,k}\, \delta^2}{\sqrt{(2\pi w^2)^2}} - \text{FWC} \tag{55}$$

where $\sqrt{(2\pi w^2)^2}$ is the PSF's maximum value (center). Pixel saturation can occur in the same way, by reaching FWC for a pixel, but this is uncommon for space objects relevant to SSA. Instead, the gain for a camera can be set too high, so when the analog-to-digital conversion occurs, the pixels bit depth, BD, is reached. This saturation makes photometry impossible and can have unpredictable affects on astrometry, but does not lead to bleeding. Similar to (55), the constraint to avoid saturating relevant pixels is

$$g_s(t_{I,k}, G) = \frac{G\, QE\, F\, t_{I,k}\, \delta^2}{\sqrt{(2\pi w^2)^2}} - \text{BD} \tag{56}$$

where F is the brightness of either the space object being tracked or the brightest possible space object. Note that the negative effect of saturation on astrometry may not be sufficient to always require this constraint, but that is case dependent.

B. Star Field Clutter

In many cases of SSA missions, the intuitive tasking involves rate tracking a space object. Intuitively, the reward functions in this paper often prioritize longer exposure times. The reason exposure time is often not maximized is due to star field clutter. Rate tracking an object causes stars to streak through an image, and when many stars are present this can clutter a large percentage of the image. Methods exist to subtract out the stars and preserve data on other light sources [24] but because star photons are a Poisson process, they still lead to large spikes in uncertainty, especially in photometry. Furthermore, SSA missions often detect previously unknown objects as uncorrelated tracks (UCT); with high levels of star clutter this becomes difficult.

This constraint is formulated as a maximum acceptable percentage of pixels obfuscated by stars, $\%_{\text{max}}$.

$$l = \frac{t_{I,k}\dot{\theta}}{\text{iFoV}} \tag{57}$$

$$N_{\text{star}} = \#_{\text{star}}(9\pi w^2 + 6lw) \tag{58}$$

$$g_{\%}(t_{I,k}, \dot{\theta}) = \frac{N_{\text{px}}}{N_{\text{total}}} - \%_{\text{max}} \tag{59}$$

where l is the length of star streaks in the image, $\dot{\theta}$ is the tracking rate, $\#_{\text{star}}$ is the number of star in the field of view, w is the standard deviation of the point spread function, and N_{total} is the total number of pixels in the image.

C. Probability of Detection

An important consideration is the probability of detection of an object. This idea can be used as two possible constraints, one on detecting a specific object of interest and one on detecting various objects of opportunity in the background. Object of opportunity refers to an object which may unexpectedly pass through the field of view during a data campaign. SSA missions often desire that as many objects as possible be detected and characterized to increase overall situational awareness. Mathematically, this objective is best quantified as the total photometric evidence for an object, while considering the total corruption of that evidence by noise. This is then measured through total photometric SNR of an object in a particular image

$$\text{SNR}\left(\sum z_i\right) = \frac{\mathbb{E}\left[\sum z_i\right]}{\sqrt{\mathbb{E}\left[\left(\left[\sum z_i\right] - \mathbb{E}\left[\sum z_i\right]\right)^2\right]}} \tag{60}$$

$$\approx \frac{GQ\bar{F}t_I}{\sqrt{N_k}\sigma} \tag{61}$$

which encapsulates in one number the ratio of information to corruption. Note that $GQ\bar{F}t_I$ is the sum of (15) over all pixels for a given time step and N_k is the number of pixels over which the signal is spread. The number of pixels N_k is dependent on the size of the point spread function and the length over which the object streaks. For tracking a known object, this number is already calculated for the summations in the information equations while for objects of opportunity this is inherently unknown. For objects of opportunity a nominal value must be chosen for N_k. This gives an equality constraint of

$$g_{\text{SNR}}(t_{I,k}) = \text{SNR}_{\text{min}} - \text{SNR}\left(\sum z_i\right) \tag{62}$$

where SNR_{min} is some minimum value of SNR, dependent on the detection method being used. An aggressive minimum SNR would be 3, which pushes the limits of current detection methods [21].

D. Side Constraints

Many of the design variables have side constraints which may be considered.

$$t_{I,\text{min}} \leq t_{I,k} \leq t_{I,\text{max}} \tag{63}$$

$$g_{\text{FoR}}(\alpha, \delta) \leq 0 \tag{64}$$

$$g_{\text{slew}}(\dot{\alpha}, \dot{\delta}) \leq 0 \tag{65}$$

In (63), integration time is usually bounded by minimum and maximum values which are dependent on the specific camera itself. In (64), observatories sometimes have physical constraints on what azimuth and elevation angle pairs are achievable, which again can be used on a case by case basis. In (65), the telescope mount may require a constraint on slew rate, which is dependent on the mount in question. The constraint must be tailored to each sensor mount, and may not be necessary for campaigns involving slow moving objects.

V. Optimization Techniques

This section discusses how to calculate gradients on the various reward functions, how to treat some of the design variables, and what optimization methods are used in this work.

A. Gradients

This section develops gradients for the reward functions with respect to the timing vector, $\mathbf{t}_I$. The gradients here are only shown for the simpler stationary point spread function, while the more complicated moving point spread function gradients are shown in Appendix A. In order to efficiently search for optima, it is useful to have analytic gradients of the reward functions with respect to the integration time vector. Before proceeding, note the derivatives of the integration time and center times from (1) and (2) for the exposures

$$\frac{\partial t_{I,k}}{\partial t_k} = -1, \qquad \frac{\partial t_{I,k}}{\partial t_{k-1}} = 1 \tag{66}$$

$$\frac{\partial \bar{t}_k}{\partial t_k} = 1/2, \qquad \frac{\partial \bar{t}_k}{\partial t_{k-1}} = 1/2 \tag{67}$$

For spatial information, (22) must be expanded using (15) and (10),

$$\frac{\partial I_{xx}}{\partial t_k} = \frac{\partial}{\partial t_k}\left(\frac{BF^2}{F_o w^4}\sum_k t_{I,k}\sum_i \xi_{i,k}^2 h_{i,k}^2\right) \tag{68}$$

where $t_{I,k}$ is defined in (1). The differentiation results in

$$\frac{\partial I_{xx}}{\partial t_k} = \frac{BF^2}{F_o w^4}\left(\sum_i \xi_{i,k}^2 h_{i,k}^2 - \sum_i \xi_{i,k-1}^2 h_{i,k-1}^2\right). \tag{69}$$

This equation represents the trade-off between lengthening the $k-1$th integration while shortening the kth integration. Consequently, if the shape of the point spread function is constant from frame to frame, the two summations yield a derivative of zero. This implies for astrometric position information, when the exposure is taken does not matter, only the amount of exposure; if, say, 20 seconds of exposure will be taken this time can be spread between any number of measurements of any lengths and achieve equal information. In realistic circumstances, the presence of dead time implies that longer exposure times are better, as less time is wasted.

Similarly for the velocity astrometry information,

$$\begin{aligned}\frac{\partial I_{\dot{x}\dot{x}}}{\partial t_k} &= \frac{\partial}{\partial t_k}\frac{BF^2}{F_o w^4}\sum_k t_{I,k}(\bar{t}_k - t^*)^2 \sum_i \xi_{i,k}^2 h_{i,k}^2 \\ &= \frac{BF^2}{F_o w^4}\Big(t_{I,k}(\bar{t}_k - t^*) - (\bar{t}_k - t^*)^2\Big)\sum_i \xi_{i,k}^2 h_{i,k}^2 \\ &-\Big(t_{I,k-1}(\bar{t}_{k-1} - t^*) - (\bar{t}_{k-1} - t^*)^2\Big)\sum_i \xi_{i,k-1}^2 h_{i,k-1}^2\end{aligned} \tag{70}$$

where $\bar{t}_k$ is defined in (2). This equation contains an interesting interplay which provides qualitative insight on velocity astrometry. The $-(\bar{t}_k - t^*)^2$ term, which is always negative for the t_k integration and positive for the t_{k-1} integration, represents the increasing t_k will reduce one exposure time while increasing another. Conversely, the $t_{I,k}(\bar{t}_k - t^*)$ term tends to push the t_k away from t^* to maximize the baseline. These two parts of the gradient oppose each other the optimum lies somewhere in between.

The photometry information gradient is more complicated due to the various instances of $t_{I,k}$ in the denominator, but it is calculable. First note the expanded version of I_{FF},

$$\begin{aligned} I_{FF} &= B^2 \sum_k \sum_i \frac{t_{I,k}^2 h_{i,k}^2}{BF_o t_{I,k} + B^2 t_{I,k}^2 h_{i,k}^2 \alpha_k^2/2} \\ &= B \sum_k \sum_i \frac{t_{I,k} h_{i,k}^2}{F_o + B t_{I,k} h_{i,k}^2 \alpha_k^2/2} \end{aligned} \tag{71}$$

where α_k is dependent on $t_{I,k}$. The derivative of this expression with respect to t_k is then a function of the kth and $k-1$th time steps,

$$\begin{aligned} \frac{\partial I_{FF}}{\partial t_k} &= B^3 \sum_i \frac{-t_{I,k}^2 h_{i,k}^2}{\text{Var}(z_{i,k})^2} \left(F_o + B t_{I,k}^2 h_{i,k}^2 \alpha_k \frac{\partial \alpha_k}{\partial t_k} \right) \\ &- B^3 \sum_i \frac{-t_{I,k-1}^2 h_{i,k-1}^2}{\text{Var}(z_{i,k-1})^2} \left(F_o - B t_{I,k-1}^2 h_{i,k-1}^2 \alpha_{k-1} \frac{\partial \alpha_{k-1}}{\partial t_k} \right) \end{aligned} \tag{72}$$

where the derivative of α_k is

$$\begin{aligned} \frac{\partial \alpha_k}{\partial t_k} &= A \left(\frac{1}{t_{I,k}} \cos\left(\frac{\omega t_{I,k}}{2} \right) - \frac{2}{\omega t_{I,k}^2} \sin\left(\frac{\omega t_{I,k}}{2} \right) \right) \\ &= \frac{A}{t_{I,k}} \left(\cos\left(\frac{\omega t_{I,k}}{2} \right) - 1 \right) + \frac{\alpha_k}{t_{I,k}} \end{aligned} \tag{73}$$

This gradient gives less intuition than the previous ones. In practice its performance depends on α as to whether it tries to drive the exposures to be small or large.

B. Karush Kuhn Tucker Conditions

Many optimization problems with analytic gradients can be solved analytically. In the general case allowing for constraints, the Karush-Kuhn-Tucker conditions are a series of equations which provide a framework for analytic solutions [25]. The basis of such an analysis involves setting the gradient of the reward function equal to zero and solving for the design variables. Such an analysis on (69) gives

$$\sum_i \xi_{i,k}^2 h_{i,k}^2 = \sum_i \xi_{i,k-1}^2 h_{i,k-1}^2 \tag{74}$$

which is not a function of the design variables and in general always true. Assuming the above equality holds, the velocity information in (70) gives

$$\begin{aligned} &t_{I,k}(\bar{t}_k - t^*) - (\bar{t}_k - t^*)^2 \\ &\quad = t_{I,k-1}(\bar{t}_{k-1} - t^*) - (\bar{t}_{k-1} - t^*)^2 \end{aligned} \tag{75}$$

which is an equation with three unknowns, t_{k-1}, t_k, and t_{k+1}. The full gradient gives one equation for every unknown and is therefore solvable, though non-linearity may provide multiple solutions. The photometry information gradient is much more complicated, due to multiple instances of $t_{I,k}$ in the gradient numerator and denominator. Furthermore, in Appendix A gradients for the more general streaking versions of these reward functions are shown. Finally, though the constraints discussed in Section IV may not be active in many of the simulations, their inclusion implies the need for a Lagrange multiplier analysis. Due to the complicated nature of these gradients and the ultimate desire for Pareto type analysis, this paper does not spend any further time discussing analytic optimization solutions. The prospect of further analysis here marks a potent area for future work.

C. Optimization Methods

The primary optimization method used in this work is a descent method. Because analytic gradients exist, this is an efficient method which reliably solves the optimization problem. In practice, the optimization seems well posed with no problems involving discrete variables, poorly posed constraints, or local minima. Constraints are handled with an exterior penalty function which is easy to implement and has shown no problems in practice [25]. The time vector is of a variable length, which corresponds to different numbers of exposure times. This is currently solved by running the optimization for all possible lengths, N_t, and choosing the solution with the best reward. There may be ways to solve this more efficiently, which should be explored in future work.

The multi-objective problem is well posed and can be solved with a simple weighted sum method [25]. The actual Pareto surface is typically non-convex, but the Pareto surface for a fixed value of N_t appears convex in practice. The weighted sum method gives well posed Pareto surfaces for each value of N_t and the resulting series of Pareto surfaces are combined into a single final surface. This can be seen in the follow results section in Figures 16 and 18.

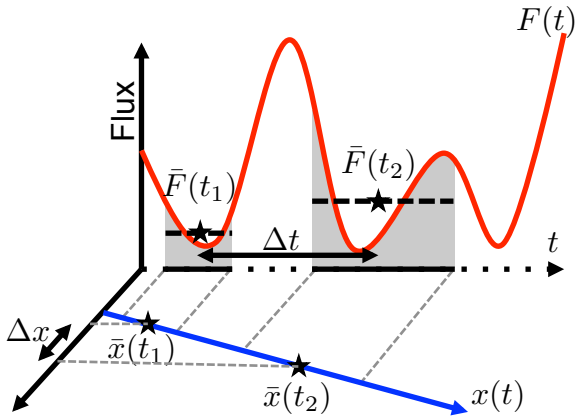

Fig. 5. Astrometry gets more information from long exposure times, and a long time baseline. Photometry gets more information from short exposure times, to reduce uncertainty from time varying signals.

TABLE I
OBSERVATION CAMPAIGN PARAMETERS

G	Q	F_o	δ	w
1.0	1.0	100. ph/(s px^2)	1.0 px	1.5 px
Total time	t_d	Mean Flux	ω	A
20 s	0.5 s	1000 ph/s	$\pi/4$ rad/s	10, 100 ph/s

VI. OPTIMAL SOLUTIONS FOR TELESCOPE CONTROL

A. Discussion and Analysis of Reward Functions

This section gives an intuitive explanation of the various reward functions developed in this paper. The main design variables that affect the image information content are the exposure times. Figure 5 illustrates the interplay of photometry and astrometry. Figure 5 shows two exposures centered at two times, t_1 and t_2, and how they appear with respect to both position and brightness. Exposure time in an image is generally proportional to information content, and so t_2 provides more raw position and brightness information. This is exactly true for position astrometry, but velocity astrometry is dependent on both Δx and Δt as well so separating two long exposures is also useful. Constant flux photometry would also want long exposures, but the curvature of $F(t)$ in Figure 5 shows why long exposures are a liability due to the potential bias.

In the next few subsections, the reward functions and subsequent Pareto surfaces are explored over a particular nominal test case. The test case has parameters defined in Table I. Total time refers to the total length of the campaign and is equivalent to the final element of the exposure time vector, t_{N_t+1}. The primary design variable being explored is the exposure time vector. The slew variable is simplified as object speed (px/s) and object heading (degrees) in the pixel plane, though the object speed is set to zero for many of these simulations to maximize the intuition in the results. Gain, G, quantum efficiency, Q, and PSF size, w, play only a small role in information content and are set to be round values to minimize their impact. The flux, background noise, and amplitude are chosen as nominal values. The relative values of A (sinosoid amplitude) and F_o (background noise flux) tend to determine whether photometry prioritizes avoiding bias through ϵ_F versus raw number of photons. Two values of A are used in the simulation section so each case can be separately analyzed.

Before fully analyzing the reward functions, the aliasing error discussed in Section III is validated here. Measurement values are all generated by generating actual streaks (with no noise) and summing up the pixels. For a the time span and parameters defined in Table I, the different exposure times are shown in Figure 6. The exposures have three different lengths, one well above the Nyquist frequency, one which experiences high levels of aliasing, and one with only small errors.

The velocity cost function pushes exposure center time $\bar{t}_k$ away from the campaign center time, t^*. This results in a single exposure that occurs over the entire time span which necessitates $\bar{t}_k = t^*$ and zero information. Furthermore, while the parameter t^* is set as the center time of the campaign, as this is typically when velocity is estimated, it could be set to other values which can give very different answers. These examples highlight the limitations of the above analysis; the reward functions are the trace of a single part of the Fisher information matrix, don't account for nuisance parameters and don't account for every possible factor. The reward functions are surrogates to actual information and have a good deal of room for improvement.

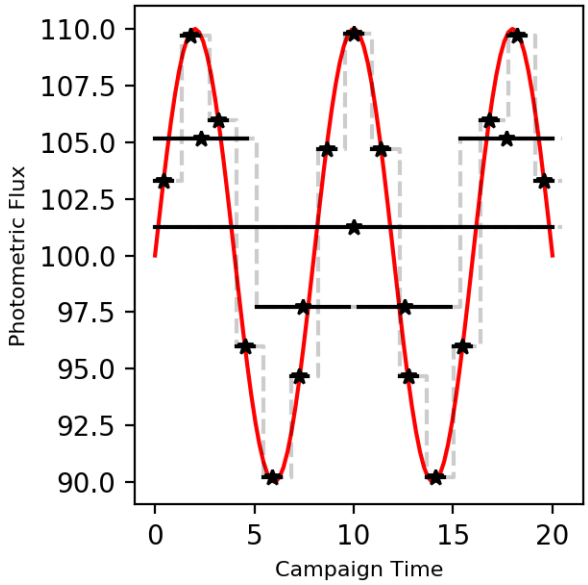

Fig. 6. Flux over time as measured by different exposure times. The smooth red line is truth while the solid black lines represent measured flux for exposure times of $t_{I,k} = 20$s, $t_{I,k} = 4.6$s, and $t_{I,k} = 0.86$s. Stars are paced at the center time of each exposure, $\bar{t}_k$.

B. Optimal Velocity Astrometry Solution

More photons lead to better statistical significance for position astrometry in an image or series of images. For velocity astrometry, more photons still help, but the time baseline over which observations are taken is important as well. This leads to prioritizing long exposure times in the first and last observation of an image set. There is a natural counterweight to this, because longer first and last exposure times push the first and last center times, $\bar{t}_k$ closer towards the center. As mentioned, the optimal arrangement of exposure times is solved with a descent algorithm, which is performed over a range of values for the number of exposure times, N_t. Because each number of exposures is solved independently, each solution can be shown and respectively analyzed. In Figure 7, each solution integration set is visually represented. Most of the solutions regardless of N_t have the same general form, prioritizing the first and last exposure. As (23) implies, the integrations furthest away from the center time, $t^* = 10$s, have the most information value. This is better illustrated in Figure 8 which shows the cumulative information after each exposure as a function of time. The integrations very close to 10s have little impact on the information content, and morph to support maximizing information from the first and last integrations. This leads to all of the solutions with more than 4 integrations having similar first and last integrations, while the integrations in the middle of the set vary greatly. The information content in each solution in Figure 7 is shown in Figure 9. Note how the information content for all solutions past 6 exposures is effectively the same. Figure 9 also compares the solutions to campaigns of constant exposures, to illustrate the advantages.

C. Optimal Photometry Solution

Constant flux photometry requires maximizing the number of photons, similar to position astrometry, and therefore wants a long exposure time. Contrary to the other reward functions, photometry on a variable flux signal requires sufficiently short exposure times in order to minimize the flux bias, ϵ_F. This requirement creates a reward function that wants both short exposures and as little dead time as possible. To highlight the duality of this reward function, Figure 10 shows solutions for $A = 100$, while Figure 13 shows solutions for $A = 10$. In general there is no reason to vary the exposure time so the solutions typically have constant t_I. Figure 10 illustrates why this is in the solutions for a low number of exposures; the solution involves minimizing as many exposures as possible and leaving one large exposure with a large photometry bias. The primary difference between $A = 100$ and $A = 10$ is the optimal exposure time. The integration time in the solution does not have intuitive meaning without the context provided by the frequency of the oscillating flux. The choice of integration time combined with $\omega = \pi/4$ gives a value on Figure 4, associating with a certain amount of error. Figure 13 is skewed towards ignoring the variable flux and prioritizing as few exposures as possible, and so the solution occurs as 4 integrations of about 4.5 seconds each with $\alpha = 0.44A$. Figure 10 is skewed towards prioritizing the variable flux as a large source of error, and so the solution occurs as 8 integrations of about 2.0 seconds each with $\alpha = 0.10A$. Recall that the value of α directly defines the variance in (39), which is in the denominator of (45). The optimization chooses values of t_I only in that they directly define the error due to ϵ_F. Figures 11 and 14 show the information over time for the optimal campaign, which takes the form of

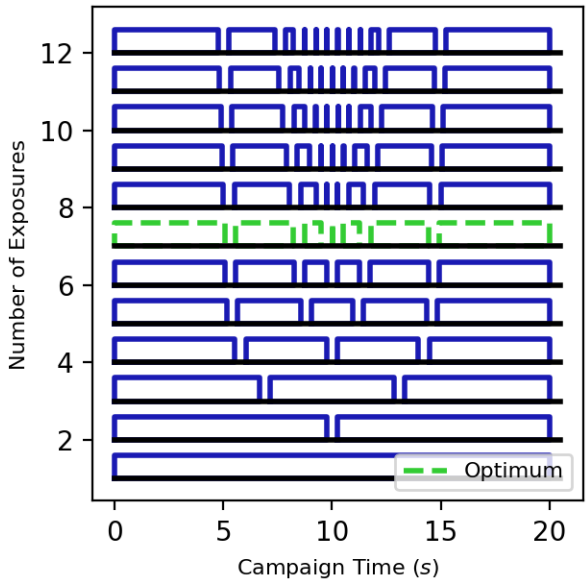

Fig. 7. For the velocity information reward function, this shows each optimal set of integrations for a respective total number of integrations. The total number of integration which provides the highest reward is highlighted with a green dashed line.

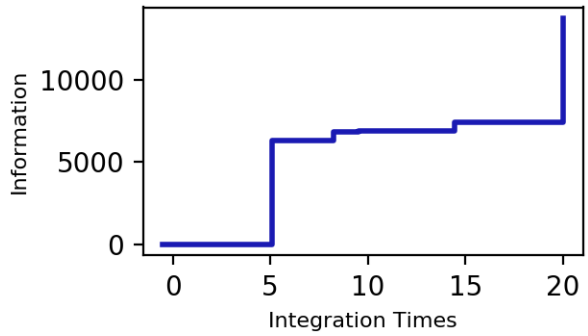

Fig. 8. For the velocity information reward function, this shows the cumulative information over time for the optimal solution. Information is focused in the first and last exposures.

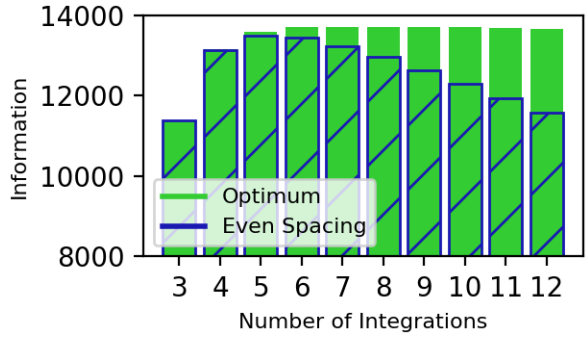

Fig. 9. For the velocity information reward function, this shows the information content for each possible number of integrations (value of N_t). Information is shown for a constant exposure time at each value of N_t for comparison.

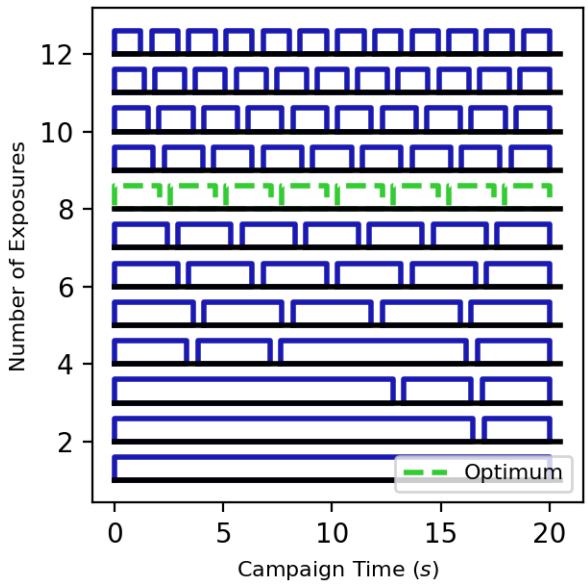

Fig. 10. For the photometry information reward function and $A = 100$, this shows each optimal set of integrations for a respective total number of integrations. The over all optimum is highlighted with a green dashed line.

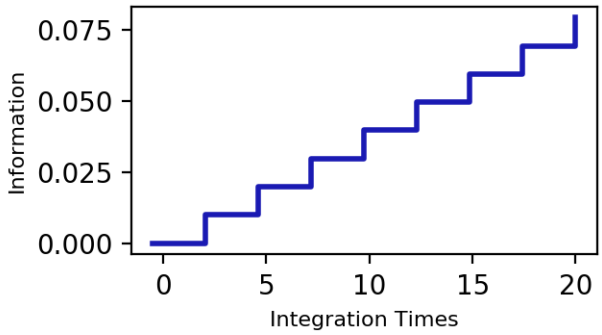

Fig. 11. For the photometry information reward function and $A = 100$, this shows the cumulative information over time for the optimal solution. Information is focused in the first and last exposures.

a simple step pattern. Figures 12 and 15 show the information for each exposure time compared against a constant exposure time campaign. The two only diverge for low numbers of exposures corresponding with the non constant exposure campaigns in Figures 10 and 13.

D. Velocity Astrometry Versus Photometry Pareto Surface

Because this is multi-objective optimization, there is no single solution but a set of solutions which all attempt to balance the two reward functions. This set of solutions can be seen in Figures 16 and 18, for $A = 100$ and $A = 10$ respectively, as a curve through the space defined by the two reward functions. Because the rewards have different units, both solutions are normalized by the individual optima for each reward function. This set of individual optima is known as the utopia point. As discussed in Section V, the actual Pareto Surfaces are composed of a series of visually convex surfaces corresponding to different numbers of exposures, N_t. The surface in Figure 16 goes from $N_t = 8$ to $N_t = 7$ to $N_t = 6$ and then back to $N_t = 7$ for the very last few solutions, though it is hard to distinguish visually. The surface in Figure 18 is comprised of a series f disjoint surfaces from $N_t = 4$ to $N_t = 7$. To complement the Pareto surfaces, a series of solutions along the Pareto frontier are provided in Figures 17 and 19. These solutions show the steady progression between a velocity astrometry optimal solution in Figure 7 at the bottom to a photometry optimal solution in Figures 10 and 13 at the top. To provide context for a single solution, the solution closest to the utopia point, $[1, 1]^T$, in terms of Euclidean distance is highlighted on all plots. The highlighted solutions in the middle of Figures 17 and 19 provide a campaign which intuitively balances photometry and astrometry by taking the optimal first and last integrations for astrometry and inserting the optimal photometry tasking in between.

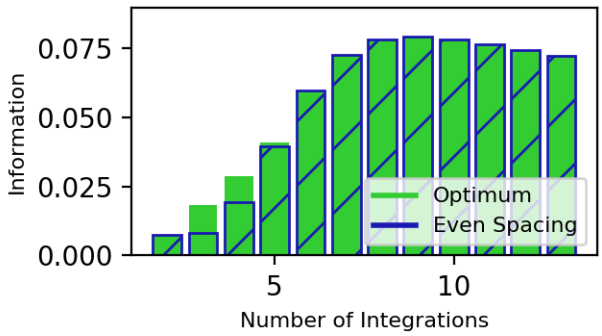

Fig. 12. For the photometry information reward function and $A = 100$, this shows the information content for each possible number of integrations (value of N_t). Information is shown for a constant exposure time at each value of N_t for comparison.

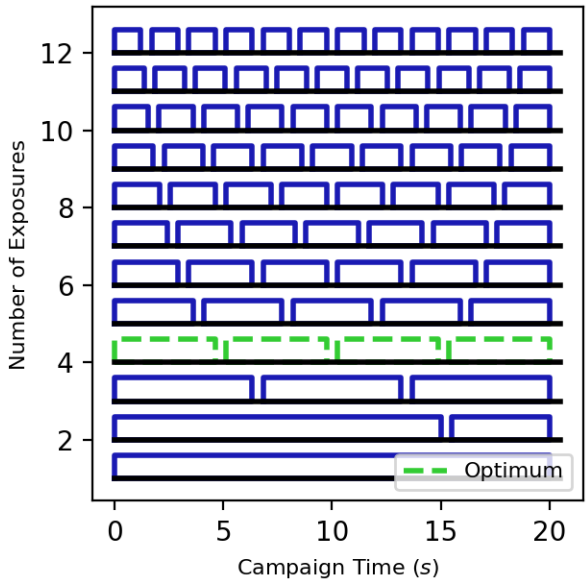

Fig. 13. For the photometry information reward function and $A = 10$, this shows each optimal set of integrations for a respective total number of integrations. The over all optimum is highlighted with a green dashed line.

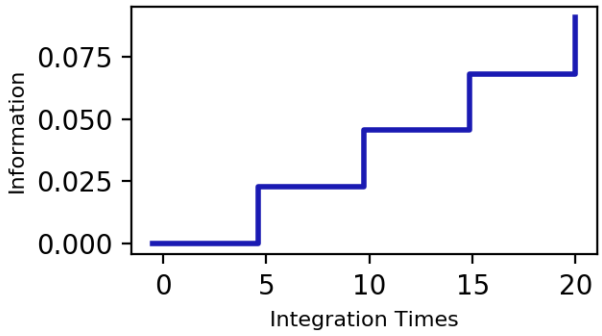

Fig. 14. For the photometry information reward function and $A = 10$, this shows the cumulative information over time for the optimal solution. Information is focused in the first and last exposures.

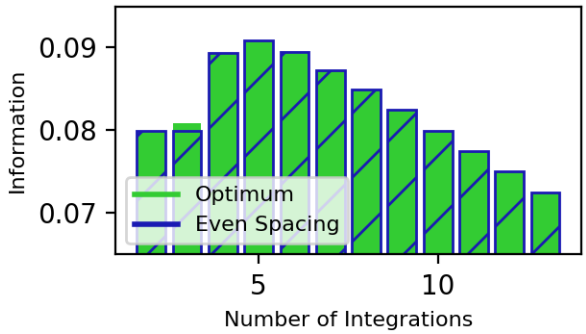

Fig. 15. For the photometry information reward function and $A = 10$, this shows the information content for each possible number of integrations (value of N_t). Information is shown for a constant exposure time at each value of N_t for comparison.

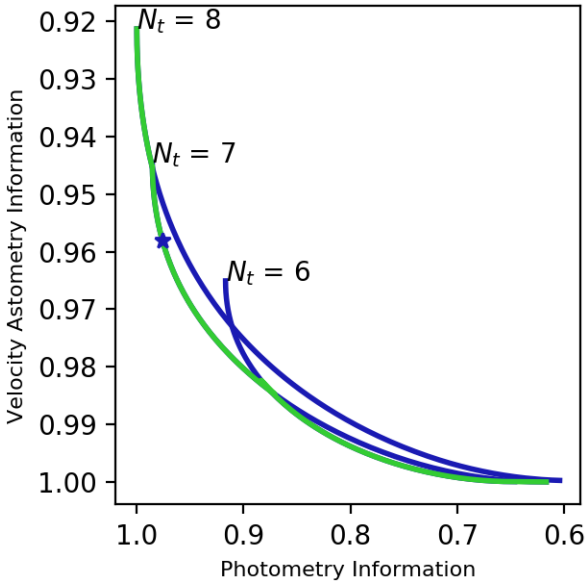

Fig. 16. Demonstration of the Pareto surface between velocity astrometry and photomtery reward functions for $A = 100$. The axes are normalized by the individual optima for each reward function, or utopia point.

VII. Conclusion

This paper provides a framework for analyzing how to select telescope parameters for SSA data collection. Reward functions are developed for the primary two goals of SSA, astrometry and photometry. Gradients are developed with respect to the main design variable considered, exposure time. This provides results for an optimal exposure time schedule and Pareto frontiers between the two reward functions.

One of the main lessons from this work is the trade-off between the various reward functions Photometry comes in two varieties, long exposures on an unchanging flux versus high frame rate of varying flux. Velocity astrometry by itself has an trade-off between long exposures and maximization of the time baseline. When combined together, the various reward functions can have unexpected interconnections as well, which is shown in their Pareto surfaces. While many data campaigns with a single goal may stay the same, taking data efficiently will always have value, which is the purpose of this work.

A. Limitations of Method

The primary limitation discovered in this work is creating a reward function for velocity astrometry. The inclusion of the t^* parameter is less than intuitive and the current solution gives zero information for a stationary object in a single object. This unintuitive result forms an avenue for future work. There are a variety of other factors which can cause uncertainty in the estimate and would therefore reduce information content, such as pointing and slewing error. There are also more design variables which could be analyzed such as the ability to dynamically window and bin images. The main limitation is, by adding more design variables, factors, and constraints the analysis becomes more complex and intuitive results are hard to obtain.

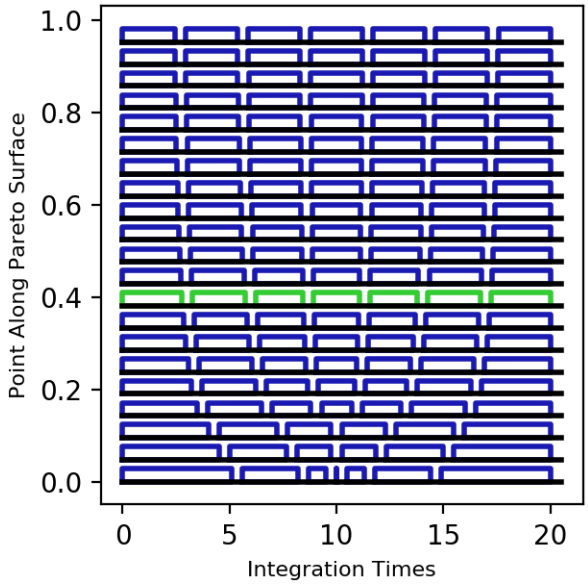

Fig. 17. Each optimal set of integrations for a respective point along the Pareto surface for $A = 100$. Solutions vary from the optimal velocity solution in Figure 7 to the optimal photometry solution in Figure 10.

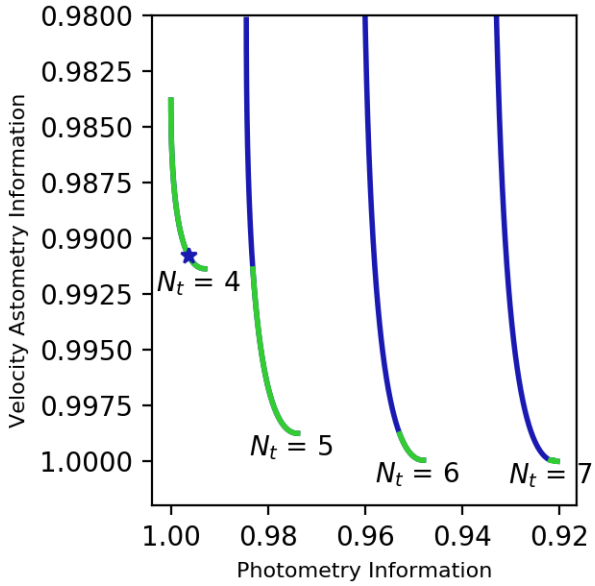

Fig. 18. Demonstration of the Pareto surface between velocity astrometry and photomtery reward functions for $A = 10$. The axes are normalized by the individual optima for each reward function, or utopia point.

B. Opportunities for Future Work

This paper has spawned a variety of exciting areas of future work.

The reward function gradients and optimization results are all centered on the exposure time vector as the primary design variable. Some minor analysis has been performed on slew rate which lead to the intuitive result that rate tracking generally leads to better information. The primary results treat slew rate as a fixed variable determined by the feasibility of rate tracking. Especially when considering some constraints such as star clutter and reliability of star identification, there may be interesting situations when choosing a non-rate track trajectory could be advantageous. Another variable which is not discussed in detail in this paper is the ability of modern sensors to sample a smaller "window" inside an image, or sub-sample blocks of pixels into single pixels. These processes, known as windowing and binning, provide a way to exchange data quality for data down-link rate. In the case of wanting high frame rate data, an interesting case can be made to include these processes as full design

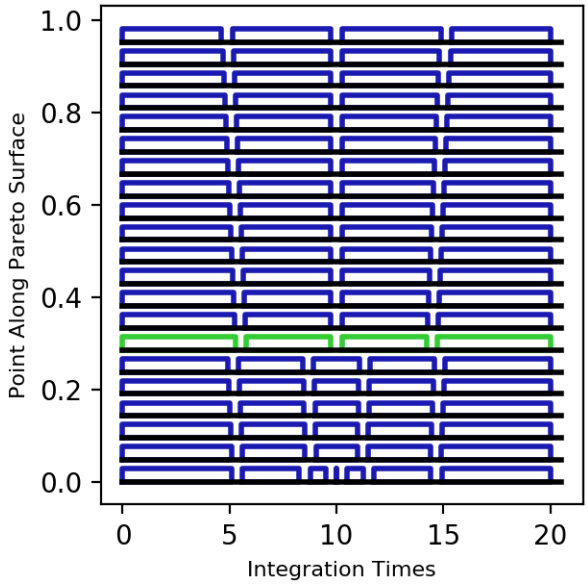

Fig. 19. Each optimal set of integrations for a respective point along the Pareto surface for $A = 10$. Solutions vary from the optimal velocity solution in Figure 7 to the optimal photometry solution in Figure 13.

variables. Related to windowing and binning is the pointing uncertainty of a telescope, which is typically found through star identification. Not only could this inherently have an affect on the various information metrics, but it is dependent on factors such as slew rate, field of view, and astrometry information of stars.

The results in this paper are rather theoretical, providing a framework of how to design data campaigns with only minimal analysis of the actual data campaigns. Part of the on going and future work associated with this work is validation on simulated and actual data campaigns. While the rewards functions here are based on the maximum likelihood estimator, there are a variety of detection, tracking and estimation techniques for both astrometry and photometry. Data can take a variety of forms depending on telescope field of view, aperture, location, etc. An extensive set of validations would be best to explore how the reward functions in this paper and future reward functions perform.

In the case of a signal with a known frequency or already well known light curve, the only engineering decision is choosing what point on the Pareto surface is desired. This is complicated when the signal frequency and amplitude are unknown. Furthermore, signals may not be sinusoidal in shape and can have interesting artifacts such as glints. This paper sidesteps this design decision by selecting a worst case scenario frequency and amplitude and solving accordingly. The intuitive result for such a situation is to initially have exposure times as short as possible to allow dynamic estimation of frequency content, then switch to a Pareto solution suitable to the detected frequency. This is at odds with the astrometry which calls for starting the campaign with a single long exposure. Solving these issues with a dynamic algorithm that updates its solution based on new data provides a wealth of new engineering problems.

As of right now, the velocity astrometry reward function registers zero information for a single rate tracking image, and has a problematic parameter, t^*. Further analysis into how to develop velocity astrometry may provide an easy intuitive solution to this. The current astrometry rewards assume that position and velocity information are the only realistic objectives. However, given a long enough campaign, full orbit information becomes observable. Future work should therefore look at how to extend or replace the astrometry reward functions with one which maximizes information on full orbit determination. Photometry, similarly, is solved in a simplistic way right now by attempting to minimize the uncertainty of the flux over time. In reality, photometry is part of a broader problem of object classification, whose objectives may require a wholely new reward function or functions. All of the reward functions developed in this paper should not be viewed as final results, but instead as a blueprint on how to develop a reward function for whatever specific objects are necessary in a given situation. It is the authors hope that this work spawns a multitude of follow on projects analyzing new ways to maximize SSA data.

APPENDIX
VARIOUS GRADIENT FORMULATIONS

A. Position Gradient on Streak

Position information on a streak object can be reformulated to give

$$\frac{\partial I_{xx}}{\partial t_k} = \frac{\partial}{\partial t_k}\left(\frac{BF^2}{F_o w^4}\sum_k \frac{1}{t_{I,k}}\sum_i C_{i,k}^2\right) \tag{76}$$

with

$$C_{i,k} = \int_{t_k}^{t_{k+1}-t_d} \xi_i(t)h_i(t)\mathrm{d}t \tag{77}$$

Included for notation ease. This leads to

$$\begin{aligned}\frac{\partial I_{xx}}{\partial t_k} =& \frac{BF^2}{F_o w^4}\left(\sum_i \frac{C_{i,k}^2}{t_{I,k}^2} - \frac{2C_{i,k}}{t_{I,k}}\xi_i(t_k)h_i(t_k)\right.\\ &\left. - \sum_i \frac{C_{i,k-1}^2}{t_{I,k-1}^2} - \frac{2C_{i,k-1}}{t_{I,k-1}}\xi_i(t_k-t_d)h_i(t_k-t_d)\right)\end{aligned} \tag{78}$$

where $t_{I,k}$ is defined in (1). Similarly for velocity astrometry,

$$\begin{aligned}I_{\dot{x}\dot{x}} &= \frac{BF^2}{F_o w^4}\sum_k \frac{1}{t_{I,k}}\sum_i D_{i,k}^2\\ \frac{\partial I_{\dot{x}\dot{x}}}{\partial t_k} &= \frac{BF^2}{F_o w^4}\left(\sum_i \frac{D_{i,k}^2}{t_{I,k}^2} - \frac{2D_{i,k}}{t_{I,k}}d_i(t_k)\right.\\ &\left. - \sum_i \frac{D_{i,k-1}^2}{t_{I,k-1}^2} - \frac{2D_{i,k-1}}{t_{I,k-1}}d_i(t_k-t_d)\right)\end{aligned} \tag{79}$$

where

$$D_{i,k} = \int_{t_k}^{t_{k+1}-t_d} \xi_i(t)h_i(t)(t-t^*)\mathrm{d}t \tag{80}$$

$$d_i(t) = \xi_i(t)h_i(t)(t-t^*) \tag{81}$$

is another constant substituted for ease of notation. For both of these formulations, the information in the y direction is identical save for η replacing ξ.

For streaking photometry information

$$\begin{aligned}I_{FF} &= B^2\sum_{i,k}\frac{\left(\int_{t_k}^{t_{k+1}-t_d} h_i(t)\mathrm{d}t\right)^2}{\mathrm{Var}(z_{i,k})}\\ &= B^2\sum_{i,k}\frac{\left(\int_{t_k}^{t_{k+1}-t_d} h_i(t)\mathrm{d}t\right)^2}{BF_o t_{I,k} + B^2\alpha_k^2\int_{t_k}^{t_{k+1}-t_d} h_i(t)\mathrm{d}t}\end{aligned} \tag{82}$$

The derivative is then

$$\begin{aligned}\frac{\partial I_{FF}}{\partial t_k} =& B^2\sum_i\left(\frac{-2\mathrm{Var}(z_{i,k})E_{i,k}h_i(t_k) + E_{i,k}^2 e_{i,k}(t_k)}{\mathrm{Var}(z_{i,k})^2}\right.\\ &\left. - B^2\sum_i\frac{-2\mathrm{Var}(z_{i,k-1})E_{i,k-1}h_i(t_k-t_d) + E_{i,k-1}^2 e_{i,k}(t_k-t_d)}{\mathrm{Var}(z_{i,k-1})^2}\right.\end{aligned} \tag{83}$$

where the derivative of α_k is defined in (73) and $E_{i,k}$ and $e_{i,k}$ are

$$E_{i,k} = \int_{t_k}^{t_{k+1}-t_d} h_i(t)\mathrm{d}t \tag{84}$$

$$e_{i,k}(t) = (BF_o + B^2\alpha_k^2 E_{i,k}h_i(t) - B^2\alpha_k E_{i,k}^2\frac{\partial\alpha_k}{\partial t_k}) \tag{85}$$

Note that the (t) in $e_{i,k}$ refers to the fact that $h_i(t)$ is evaluated at a specific time, t_k for time step k and $t_k - t_d$ for times step $k-1$.

ACKNOWLEDGMENT

This research was conducted with Government support under and awarded by DoD, Air Force Office of Scientific Research, National Defense Science and Engineering Graduate (NDSEG) Fellowship, 32 CFR 168a. I would like to thank Brien Flewelling for his guidance and inspiration throughout my graduate school career. We would like to acknowledge and thank the Air Force Research Laboratory Scholars Program for supporting this project. Finally, Dr. Ryan Coder, Andris Jaunzemis, Shez Virani, Daniel Aguilar Marsillach and all past and future contributors to GT-SORT.

REFERENCES

[1] Blake, T., Sánchez, M., Krassner, J., Georgen, M., and Sundbeck, S., "Space Domain Awareness," *Advanced Maui Optical and Space Surveillance Technical Conference*, 2011.

[2] Howell, S. B., *Handbook of CCD Astronomy*, Cambridge University Press, 2006. doi:10.1017/cbo9780511807909.

[3] Massey, P. and Jacoby, G. H., "CCD data: The good, the bad, and the ugly," *Astronomical CCD observing and reduction techniques*, Vol. 23, 1992, p. 240.

[4] King, I. R., "The Profile of a Star Image," *Publications of the Astronomical Society of the Pacific*, Vol. 83, apr 1971, pp. 199. doi:10.1086/129100.

[5] Vanvliet, L. J., *Grey-scale measurements in multi-dimensional digitized images*, Ph.D. thesis, Delft University, 10 1993.

[6] Zhang, B., Zerubia, J., and Olivo-Marin, J.-C., "Gaussian approximations of fluorescence microscope point-spread function models," *Applied Optics*, Vol. 46, No. 10, mar 2007, pp. 1819. doi:10.1364/ao.46.001819.

[7] Mullikin, J. C., van Vliet, L. J., Netten, H., Boddeke, F. R., van der Feltz, G., and Young, I. T., "Methods for CCD camera characterization," *Image Acquisition and Scientific Imaging Systems*, edited by H. C. Titus and A. Waks, SPIE, may 1994. doi:10.1117/12.175165.

[8] Lindegren, L., "Photoelectric astrometry: a comparison of methods for precise image location," *International Astronomical Union Colloquium*, Vol. 48, 1978, pp. 197–217. doi:10.1017/S0252921100074157.

[9] Hagen, N. and Dereniak, E. L., "Gaussian profile estimation in two dimensions," *Applied Optics*, Vol. 47, No. 36, dec 2008, pp. 6842. doi:10.1364/ao.47.006842.

[10] Davey, S. J., Rutten, M. G., and Cheung, B., "A Comparison of Detection Performance for Several Track-before-Detect Algorithms," *EURASIP Journal on Advances in Signal Processing*, Vol. 2008, 2008, pp. 1–11. doi:10.1155/2008/428036.

[11] Fujimoto, K., Uetsuhara, M., and Yanagisawa, T., "Statistical Track-Before-Detect Methods Applied to Faint Optical Observations of Resident Space Objects," *Advanced Maui Optical and Space Surveillance Technical Conference*, 2015.

[12] Murphy, T. S., Holzinger, M. J., and Flewelling, B., "Visual Tracking Methods for Improved Sequential Image-Based Object Detection," *Journal of Guidance, Control, and Dynamics*, jul 2017, pp. 1–14. doi:10.2514/1.g002238.

[13] Sanders-Reed, J., "Maximum likelihood detection of unresolved moving targets," *IEEE Transactions on Aerospace and Electronic Systems*, Vol. 34, No. 3, jul 1998, pp. 844–859. doi:10.1109/7.705892.

[14] Linares, R., Jah, M. K., Crassidis, J. L., and Nebelecky, C. K., "Space Object Shape Characterization and Tracking Using Light Curve and Angles Data," *Journal of Guidance, Control, and Dynamics*, Vol. 37, No. 1, jan 2014, pp. 13–25. doi:10.2514/1.62986.

[15] Coder, R. D., Holzinger, M. J., and Linares, R., "Three-Degree-of-Freedom Estimation of Agile Space Objects Using Marginalized Particle Filters," *Journal of Guidance, Control, and Dynamics*, sep 2017, pp. 1–13. doi:10.2514/1.g001980.

[16] Kaasalainen, M., "Optimization Methods for Asteroid Lightcurve Inversion I. Shape Determination," *Icarus*, Vol. 153, No. 1, sep 2001, pp. 24–36. doi:10.1006/icar.2001.6673.

[17] Kaasalainen, M., "Optimization Methods for Asteroid Lightcurve Inversion II. The Complete Inverse Problem," *Icarus*, Vol. 153, No. 1, sep 2001, pp. 37–51. doi:10.1006/icar.2001.6674.

[18] Coder, R. D., Wetterer, C. J., Hamada, K. M., Holzinger, M. J., and Jah, M. K., "Inferring Active Control Mode of the Hubble Space Telescope Using Unresolved Imagery," *Journal of Guidance, Control, and Dynamics*, may 2017, pp. 1–7. doi:10.2514/1.g002223.

[19] Benezeth, Y., Jodoin, P., Emile, B., Laurent, H., and Rosenberger, C., "Review and evaluation of commonly-implemented background subtraction algorithms," *2008 19th International Conference on Pattern Recognition*, Institute of Electrical & Electronics Engineers (IEEE), dec 2008, pp. 1–4. doi:10.1109/icpr.2008.4760998.

[20] Sanson, F. and Frueh, C., "Noise Quantification in Optical Observations of Resident Space Objects for Probability of Detection and Likelihood," *AAS/AIAA Astrodynamic Specialist Conference, Vail, CO*, 2015, pp. 15–634.

[21] Murphy, T. S., Holzinger, M. J., and Flewelling, B., "Space Object Detection in Images Using Matched Filter Bank and Bayesian Update (Submitted)," *Journal of Guidance, Control, and Dynamics*, 2016.

[22] Kay, S. V., *Fundamentals of Statistical Signal Processing: Estimation Theory*, Prentice Hall, 1993.

[23] Howell, S. B., "CCD manufacturing and operation," *Handbook of CCD Astronomy*, Cambridge University Press, 2006, pp. 8–35. doi:10.1017/cbo9780511807909.004.

[24] Sease, B., Flewelling, B., and Black, J., "A class of convex optimization problems for template-based star subtraction," *26th AAS/AIAA Space Flight Mechanics Meeting*, 2016.

[25] Arora, J., *Introduction to optimum design*, Elsevier, 2004.